On the average, local and electronic structure of NASICON-type $Li_{1.3}Al_{0.3}Dy_{0.05}Ti_{1.7}(PO_4)_3$ (LADTP)

Gugulethu C. Nkala * [1,2], Sikhumbuzo M. Masina [1], Fernando D. Vila [3], John J. Rehr [3], Rudolph M. Erasmus [4], Roy P. Forbes [1], Caren Billing [1], David G. Billing [1,2]

[1] Molecular Sciences Institute, School of Chemistry, University of the Witwatersrand, Private Bag X3, Johannesburg, 2050, South Africa

[2] DSI-NRF Centre of Excellence in Strong Materials, Private Bag X3, Johannesburg, 2050, South Africa

[3] Department of Physics, University of Washington, Seattle, WA, United States

[4] Materials Physics Research Institute, School of Physics, University of the Witwatersrand, Private Bag X3, Johannesburg, 2050, South Africa

1. Introduction

- NASICON (Na Super Ionic Conductor)-type $LiTi_2(PO_4)_3$ (LTP) (space group *R*-3*c*)has been under investigation as a promising solid-state electrolyte.
- This is attributed to its possession of a 3D network of TiO_6 octahedra corner-linked to PO_4 tetrahedra that forms tunnels through which Li^+ cations can migrate.
- The focus has been on improving its ionic conductivity (10^{-7} S/cm) by tuning the tunnel size and increasing the amount of charge carriers, via aliovalent lattice site substitutions at the Ti^{4+} (12*c*) site to the order of 10^{-4} S/cm in 15% Al-doped LTP. [1, 2]

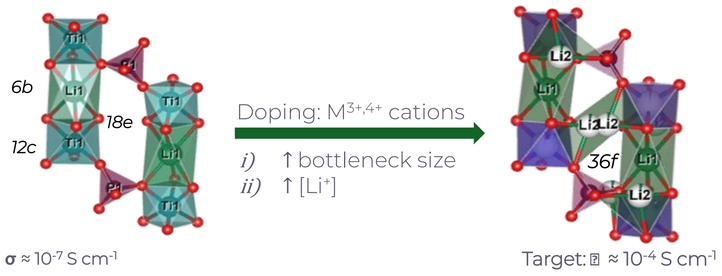

Figure 1. A closer look at the local environment of L(A)TP depicting the TiO_6 octahedra corner-linked to PO_4 tetrahedra. Li^+ occupies two sites: 6-fold oxygen coordinated M1 (*6b*), and the 8-fold oxygen coordinated M2 (*18e*). Excess Li+ added for charge balance occupy the 36*f* sites of higher stability relative to 18*e*.

Aim

- To study the average and local structure of a new 12,5% Al, 2,5% Dy co-doped LTP system, showing an improved ionic conductivity (10^{-5} S/cm).

2. Methodology

❑ Synchrotron Bragg & total scattering data

Bragg and total scattering data were measured at the 28-ID-1 (PDF) beamline at the National Synchrotron Light Source – II (NSLS-II) in transmission geometry (0,16635 Å). Rietveld and small-box modelling analyses were carried on TOPAS Academic, [3] with the structures visualized in VESTA. [4]

❑ Raman spectroscopy

Laboratory-based Raman spectra were measured using an Ar^+ laser (514 nm wavelength), with a 600 lines/mm grating and a 100 × objective lens.

❑ X-ray absorption near-edge structure (XANES)

Experimental Dy L3-edge XAS data of LADTP were measured at the 6-BM beamline at NSLS-II, using a Si (111) double crystal monochromator. Typical data reduction and linear combination fitting (LCF) analyses were carried out in the ARTEMIS package of DEMETER. [5]

❑ Theoretical approach to Dy L_3-edge XANES using FEFF10 [6]

- The optimum spectrum of Dy_2O_3 standard (*Ia*-3) symmetry, was a weighted average of two inequivalent Dy environments.
- All calculations employed an 8 Å cluster, with both electric dipole & quadrupole transitions accounted for.
- The Hedin-Lundqvist exchange-correlation potential with many-pole self-energy and a ground-state background function were used, with self-consistent field (SCF) and full multiple scattering (FMS).
- Subsequent spectra of Dy in LADTP rhombohedral (*R*-3*c*), tetragonal (*I*41/*amd*) and monoclinic ($P2_1/n$) $DyPO_4$ environments were calculated and aligned to the high-energy region of the experimental LADTP spectrum for LCF.

3. Results & Discussion

1. Average structure from synchrotron XRD (Bragg)

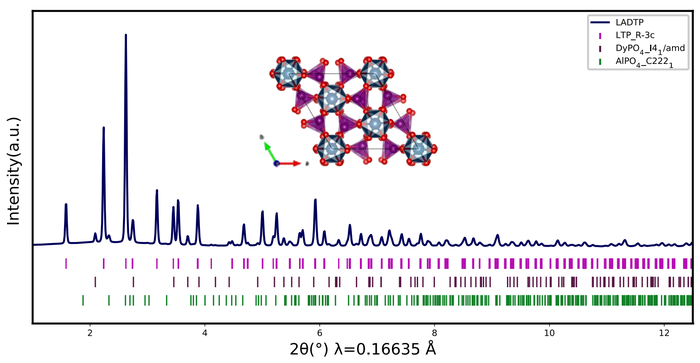

Figure 2. The room-temperature synchrotron XRD data of LADTP measured at NSLS-11. The main phase was indexed to the rhombohedral NASICON-type LTP (space group *R*-3*c*; 94,57%). Secondary phases of $DyPO_4$ (space group $I4_1/amd$; 3,30%) and $AlPO_4$ (space group $C222_1$; 2,13%) were also detected.

- Average (Bragg) structural data showed successful formation of the rhombohedral NASICON-type phase of LADTP, analogous to LTP (ICSD 95979).
- Secondary phases of $DyPO_4$ (ICSD 35705) and $AlPO_4$ (ICSD 98382) were also observed.

3. Results & Discussion

2. Average structure from Raman spectroscopy

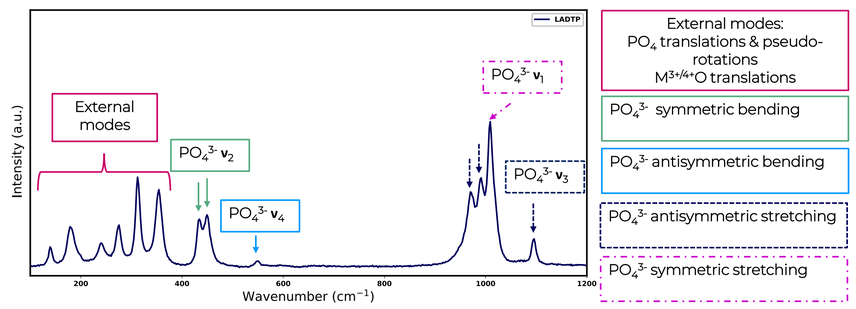

Figure 3. Raman spectrum of the Al, Dy co-doped LADTP system, indexed to the NASICON-type rhombohedral structure. [7]

- Vibrational spectrum indexed to the rhombohedral (*R*-3*c*) NASICON-type structure, similar to XRD.
- No significant account of the effect of doping on the $[Ti(PO_4)_3]$- framework.

3. Local structure from small-box modelling of the pair distribution function (PDF)

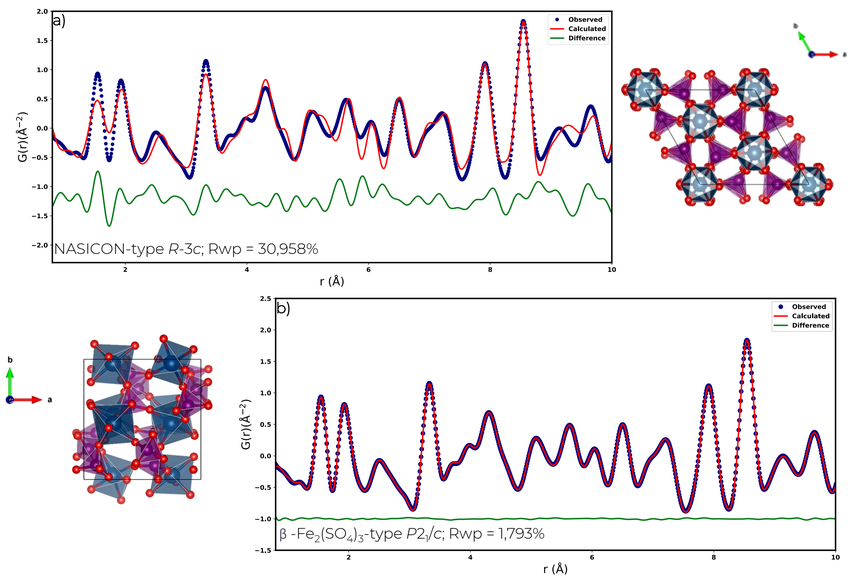

Figure 4. Small-box modelling of x-ray PDF data using (a) the rhombohedral NASICON-type *R*-3*c* from Bragg data, and (b) the monoclinic β-$Fe_2(SO_4)_3$-type $P2_1/c$ structure, [4] showing the discrepancy between average and local structure.

- Average rhombohedral structure does not account for features at $r < 10$ Å.
- Replacing Ti^{4+} with larger cations can induce monoclinic/triclinic distortions.
- Applying a monoclinic $P2_1/n$ model best describes the local structure.

4. Experimental vs Computational XANES

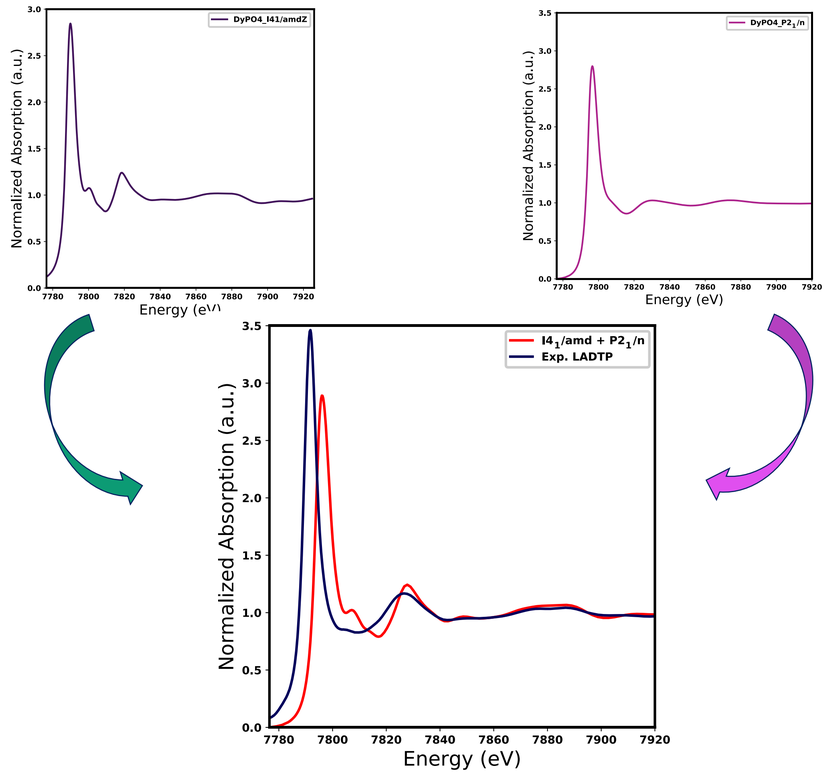

Figure 5. The Dy L_3-edge XANES showing the (a) $I4_1/amd$ model from the $DyPO_4$ secondary phase, (b) the monoclinic $P2_1/n$ model deduced from PDF small-box modelling accounting for the distorted local structure , and (c) the experimental spectrum of LADTP, with the simulated summed spectra at 86% $I4_1/amd$ + 14 % $P2_1/c$ obtained from LCF.

- The LADTP spectrum largely consists of the secondary $DyPO_4$ ($I4_1/amd$) phase computational model from Bragg; however, this model alone does not fully account for the Exp. data.
- LCF results suggest that Exp. LADTP consists of approximately 86:14 ratio of $I4_1/amd$: $P2_1/n$ models.

4. Conclusions

- The average structure of 12,5% Al, 2,5% Dy co-doped LTP system was successfully indexed to the rhombohedral NASICON-type structure (space group *R*-3*c*).
- Secondary phases of $AlPO_4$ (space group $C222_1$) and $DyPO_4$ (space group $I4_1/amd$) were observed from XRD.
- Raman spectroscopy data corroborated the rhombohedral structure observed in XRD. However, the effects of replacing Ti^{4+} with Al^{3+} and Dy^{3+} at the 12*c* site were not fully understood.
- Small-box modelling of PDF data showed a deviation of the local structure from the average rhombohedral structure. The replacement of Ti^{4+} with Dy^{3+} showed a monoclinic local structure (space group $P2_1/n$), analogous to β-$Fe_2(SO_4)_3$.
- Experimental XANES confirmed a +3 oxidation state for Dy.
- Computational XANES showed that the contribution of the secondary $DyPO_4$ phase from Bragg data, although significant, did not fully account for the observed spectrum. Including the spectrum from Dy exhibiting a monoclinic structure accounted for the spectrum reasonably well.

5. Future work

❑ Determining more accurate phase contributions of computational spectra to better reproduce the experimental data.

❑ Improve the peak broadening and white line intensity agreement between the Exp. And Comp. XANES spectra.

6. References

1. Aatiq, A., Ménétrier, M., Croguennec, L., Suard, E. and Delmas, C., 2002. On the structure of $Li_3Ti_2(PO_4)_3$. *Journal of Materials Chemistry*, *12*(10), pp.2971-2978. (DOI: 10.1039/B203652P)
2. Emery, J., Šalkus, T., Abramova, A., Barré, M. and Orliukas, A.F., 2016. NMR investigations in $Li_{1.3}Al_{0.3}Ti_{1.7}(PO_4)_3$ ceramics. Part I: structural aspect. *The Journal of Physical Chemistry C*, *120*(46), pp.26173-26186. (DOI: 10.1021/acs.jpcc.6b06764)
3. Coelho, A.A., 2018. TOPAS and TOPAS-Academic: an optimization program integrating computer algebra and crystallographic objects written in C++. *Journal of Applied Crystallography*, *51*(1), pp.210-218. (DOI: 10.1107/S1600576718000183)
4. Momma, K. and Izumi, F., 2011. VESTA 3 for three-dimensional visualization of crystal, volumetric and morphology data. *Journal of applied crystallography*, *44*(6), pp.1272-1276. (DOI: 10.1107/S0021889811038970)
5. Ravel, B. and Newville, M.A.T.H.E.N.A., 2005. ATHENA, ARTEMIS, HEPHAESTUS: data analysis for X-ray absorption spectroscopy using IFEFFIT. *Journal of synchrotron radiation*, *12*(4), pp.537-541. (DOI: 10.1107/S0909049505012719)
6. Kas, J.J., Vila, F.D. and Rehr, J.J., 2020. The FEFF code. (DOI: 10.1107/S1574870720003274)
7. Burba, C.M. and Frech, R., 2006. Vibrational spectroscopic study of lithium intercalation into $LiTi_2(PO_4)_3$. *Solid State Ionics*, *177*(17-18), pp.1489-1494. (DOI: 10.1016/j.ceramint.2011.06.025)
8. Christidis, P.C. and Rentzeperis, P.J., 1975. The crystal structure of the monoclinic $Fe_2(SO_4)_3$. Zeitschrift für Kristallographie-Crystalline Materials, 141(1-6), pp.233-245. (DOI: 10.1524/zkri.1975.141.16.233)

Acknowledgements

The author wishes to acknowledge the organizations who supported participation in the 2022 Workshop on Recent Developments in Electronic Structure:

- the US-Africa Initiative in Electronic Structure (USAfrI)
- the Innovation Fund of the American Physical Society
- Columbia University
- and the East African Institute for Fundamental Research.

The support of the DSI-NRF Centre of Excellence in Strong Materials towards this research is hereby acknowledged. Opinions expressed and conclusions arrived at, are those of the author and are not necessarily to be attributed to the CoE-SM.

This research used resources of the National Energy Research Scientific Computing Center, a DOE Office of Science User Facility supported by the Office of Science of the U.S. Department of Energy under Contract No. DE-AC02-05CH11231 using NERSC award project mp313 for 2021/2022. The NSLS-II beamlines 28-ID-1 (PDF) and 6-BM (BMM) are hereby acknowledged.